

17. Balmes, E., Corus, M., Siegert, D. (2006). Modeling thermal effects on bridge dynamic responses. In Proceedings of the 24th international modal analysis conference (IMAC-XXIV).
18. Kovalchuk, V., Onyshchenko, A., Fedorenko, O., Habrel, M., Parneta, B., Voznyak, O. et. al. (2021). A comprehensive procedure for estimating the stressed-strained state of a reinforced concrete bridge under the action of variable environmental temperatures. Eastern-European Journal of Enterprise Technologies, 2 (7 (110)), 23–30. doi: <https://doi.org/10.15587/1729-4061.2021.228960>
19. Kovalchuk, V., Hnativ, Y., Luchko, J., Sysyn, M. (2020). Study of the temperature field and the thermo-elastic state of the multilayer soil-steel structure. Roads and Bridges – Drogi i Mosty, 19 (1), 65–78. doi: <https://doi.org/10.7409/rabdim.020.004>
20. Luchko, J., Hnativ, Yu., Kovalchuk, V. (2013). Temperature field and stressed state of composite bridge span investigation. Visnyk ternopilskoho natsionalnoho tekhnichnoho universytetu, 2, 29–38.

At present, there are theoretical and experimental studies of such bearings without taking into account the elastic deformation of the bearing segments. The rotor bearings of powerful turbines at nuclear power plants are subjected to loads as high as tens of tons. One of the important issues in designing segmental bearings operating under these conditions consists in taking into account elastic deformations of the segments. A schematic diagram of a segmental hydrostatic bearing was presented and the principle of its operation was described. When determining the deformation of spherical support, a formula of change in volume of a solid steel ball subjected to uniform pressure was applied.

To determine the segment deformation in the axial direction, differential equation of bending of the strip beam as the initial one. The basic equation of deformation of rods with a curved axis acting in the plane of curvature was taken as a starting point of determining the segment deformation in the circumferential direction.

It was found in the studies that the maximum deformation of the segment is 4.5 % of radial clearance at a feed pressure of 5 MPa and can affect the bearing characteristics. A substantially nonlinear character of deformations along the segment axis was revealed. It was found that the pressure of the working fluid significantly affects the segment thickness. With an increase in feeding pressure from 1 MPa to 10 MPa, the thickness of the steel segment increased more than 2 times and the thickness of the bronze segment increased more than 3 times. It was established that the pressure of the working fluid exceeding 10 MPa substantially affects the deformation of the spherical support and the bearing clearance.

The study results will make it possible to determine more accurately the main characteristics of the segmental bearing and design it more efficiently

Keywords: *segmental bearing, segment deformation, bearing characteristics, differential equation, calculation results*

UDC 621.822.5.032:532.517.4

DOI: 10.15587/1729-4061.2021.239066

REVEALING DEFORMATION OF SEGMENTS AND THEIR SUPPORTS IN A HYDROSTATIC SEGMENTAL BEARING

Vladimir Nazin

Doctor of Technical Sciences

Department of Theoretical Mechanics,
Mechanical Engineering and Robotic
Mechanical Systems

National Aerospace University

«Kharkiv Aviation Institute»

Chkalova str., 17, Kharkiv, Ukraine, 61070

E-mail: v.nazin@khai.edu

Received date 29.06.2021

Accepted date 12.08.2021

Published date 31.08.2021

How to Cite: Nazin, V. (2021). Revealing deformation of segments and their supports in a hydrostatic segmental bearing. Eastern-European Journal of Enterprise Technologies, 4 (7 (112)), 33–40. doi: <https://doi.org/10.15587/1729-4061.2021.239066>

1. Introduction

High reliability and durability in all operating modes are some of the main requirements for bearings. In addition, the following requirements are imposed on them: guaranteed long-term working efficiency, high fire safety, good maintainability after storage, transportation, and overload.

Non-stationarity of loading, high rotational speeds of rotors, the possibility of the appearance of elastic deformations in segments, and the use of low-viscosity liquids as a lubricant are the main operating features of rotor bearings in power plant units. The high probability of turbulent flow of lubricant is caused by these factors.

Slider bearings of various types are used in existing designs of power units. There are many types of bearing shell bore.

The simplest cylindrical bore is used most often. Taking into account peculiarities of operation of rotor bearings in present-day power plant units, a bearing with self-aligning segments is the most reliable type of bearing that counteracts the excitation of vibrations. Unlike the conventional designs, it possesses stabilizing properties enabling expansion of the zone of stable rotor motion. In addition, it is able to compensate for shaft misalignments and has fewer frictional losses.

In 1972, for the first time in the practice of turbine construction, 0.3 and 0.4 m diameter segmental bearings were installed on a K-500-240 turbine (Russia). Capacities of nuclear power plants measure hundreds of megawatts, bearing diameters reach 0.8 m and more, and loads acting on bearings amount up to tens of tons. Taking into account the deformability of segments is one of the important issues in designing

segmental bearings operating in such conditions. It is especially important in designing large-diameter segmental bearings.

Thus, the need to use segmental hydrostatic bearings for rotors of high-capacity plants and the lack of information on determining deformation of segments and their supports makes relevant the study on this problem.

2. Literature review and problem statement

Journal bearings operated with the use of magnetic fluids are considered in [1]. Magnetized bearings can create fluid support through magnetostatic force. Supporting capacity provided by liquefied gas helps reduce friction. This design will be especially important in precision sliding machines. Static and dynamic characteristics of impact gas-film bearings are considered in [2]. A model of deformation of foil with a protrusion has been created using the theory of elasticity. Distribution of gas film pressure and bearing gas film thickness of the bearing and influence of parameters of the shock film structure on static and dynamic characteristics of bearing were studied based on the developed procedure. A computational model of static characteristics of self-aligning thrust bearings with an inclined pad is presented in [3]. The self-aligning thrust bearing with a tilted pad improves operational reliability by adjusting its pad by tilting a thrust ring. The kinematic model of the aligning mechanism is described. It is integrated into the existing tool of elastohydrodynamic analysis which makes it possible to forecast the load-bearing capacity of the bearing. Transient interactions between the degree of wear during sliding and liquid-solid-temperature characteristics of a sliding bearing were revealed in [4]. The journal bearing characteristics including wear rate, depth of wear, fluid pressure, contact pressure, and maximum temperature were calculated numerically. The numerical results show that the worn area is mainly located at both ends of the bearing and the time-varying profile of the worn surface can be useful in the improvement of the hydrodynamic effect. Adjustable plain bearings are considered in [5]. The most common control methods include delivery pressure control; discharge slope angle adjustment; plain bearing clearance control and lubricant viscosity control. Main problems to be solved for industrial application of adjustable plain bearings are considered. Characteristics and dynamic stability of a three-blade slider bearing with microprotrusions are considered in [6]. Some useful recommendations for future scientific studies in this area are also given in this paper. Paper [7] is devoted to experimental studies of sliding support systems. Two laboratory test procedures are presented and their ability to visualize certain bearing performance parameters is emphasized. Paper [8] briefly describes a version of the original software for analysis of hydrodynamics of cylindrical plain bearings. A two-dimensional problem of lubricant fluid flow in the bearing clearance was solved by the finite element method taking into account various types of deviation of the contact surface from cylindrical shape. A bearing design in which several zones of hydrodynamic friction are formed was considered. The influence of the base oil structure on elastic hydrodynamic friction is considered in [9]. It was found that liquids with linear molecules and flexible bonds give significantly less friction than the liquids based on molecules with spatial side groups. When using fluids based on pure ester, it has been shown that rather small differences in molecular structure can have a significant ef-

fect on bearing friction. The study [10] describes a recently developed system of base insulation that can significantly reduce lateral forces transmitted to buildings, bridges, and other structures. The system uses hydrostatic plain bearings to minimize friction between bearings and base plates. Noteworthy is study [11] in which hybrid bearings are proposed to improve in-service reliability. The bearings are a combination of rolling and film bearings. The results of theoretical and numerical studies are presented. Conditions of occurrence of the minimum friction effect have been substantiated. Article [12] presents an experimental study of a journal bearing with tilted pads. Optimized vortex grooves are made in the bearing sliding surfaces. The study results have shown that reduction of bearing surface temperature achieved by optimized vortex grooves resulted in a significant increase in bearing capacity. Thermal deformations of slider bearing pads of a powerful turbine are considered in [13]. Comparison of measurement data and calculations is given which showed good conformance for thermal deformations in pads.

A hydrostatic/hydrodynamic problem of a multi-segmental bearing with point chambers is considered in [14]. Theoretical dependences and some results of the calculation of hydrostatic/hydrodynamic forces acting on the segments are given. However, elastic deformations of the segment body and its spherical support caused by the action of these forces are not considered.

In the studies considered, there is no information on determining the deformation of segments and their spherical supports. A solution to this problem is associated with significant mathematical difficulties since it becomes necessary to jointly solve the hydrodynamic problem and determine the deformation of segments by methods of the theory of elasticity. The numerical solution of the problem under consideration is also rather complicated. Due to insufficient knowledge, as well as the prospects for the use of segmental hydrostatic bearings, it is necessary to conduct a study devoted to the analysis of deformations in the bearing segments and their supports.

3. The aim and objectives of the study

The study objective implied identifying the influence of changes in operating parameters of bearings on deformations in segments and their spherical supports. This will make it possible to more accurately determine the characteristics of bearings or establish the required thickness of their segments.

To achieve the objective, the following tasks were set:

- establish the magnitude of influence of pressure of the working fluid feed and various materials of the segment on the magnitude of its maximum deformation in circumferential and axial directions;
- determine the magnitude of influence of pressure of the working fluid feed on the minimum required thickness of the segment and establish the need of taking into account deformation of the segment supports when determining the bearing characteristics.

4. The study materials and methods

When constructing theoretical dependences for calculating the deformation of the bearing segments and their

spherical supports, methods of the theory of elasticity and strength of materials were used. To calculate deformation in the axial direction, the method of thin-walled shells was used. The segment in this direction was considered as a strip beam for which the differential equation of bending is valid. To determine deformations in the circumferential direction, an equation of determining deformations in rods with a curved axis under the action of forces in the plane of curvature was taken as the initial equation. In expressions for calculating deformations in segments, the distributed load was represented as a grid function of pressure distribution. The distributed load was assumed to be constant within the grid step.

A general solution of the differential equation describing deformations in segments in circumferential direction was found as a sum of the general solution of the homogeneous equation and a partial solution of the inhomogeneous linear equation.

To determine deformation in a spherical support of a segment, a formula of change of volume of a solid steel ball subjected to uniform pressure was used.

The developed method of calculating deformations in segments and their spherical supports was numerically implemented in the Excel program. Figures and graphs of the results obtained were constructed in the Compass graphic editor.

5. The results obtained in the study of deformations in segments and their spherical supports

5.1. Determining the segment deformation in circumferential and axial directions under the action of a distributed load on it

A schematic diagram of the segmental-type hydrostatic bearing under consideration is shown in Fig. 1.

The bearing consists of several segments 1 pivoting around spherical supports 2. The spherical support is displaced relative to the segment in the direction of rotation of the shaft 3. Working fluid is fed through holes in the spherical supports 2 and enters the supporting chambers in the working surface of the segments after passing through the system of holes in segments 1. The working fluid is fed under high pressure determined by calculation. Hydrostatic pressures

arise between the working surfaces of the segments and the shaft surface which provide the required load-bearing capacity and can cause deformation in the segments.

The posed problem of segment deformation was solved by methods of the theory of elasticity. The segment is considered loaded with an external load distributed over its surface. The segment bending will occur in two mutually perpendicular planes relative to the spherical support 2 (Fig. 1). Deformation of the spherical support 2 itself is considered as well.

When calculating deformations in the axial direction, the shell method was used. The segment was considered in this direction as a strip beam. Then the differential equation of bending of the strip beam is valid [15]:

$$\frac{E \cdot I}{1 - \nu^2} \cdot \frac{d^2 W_z}{dz^2} = M_z, \tag{1}$$

where E is the modulus of elasticity of the segment material; ν is the Poisson's ratio; M_z is bending moment; W_z is the deformation of the segment in the axial direction; I is the moment of inertia of the segment section.

Using the concept of cylindrical stiffness D , the expression (1) was transformed:

$$D \cdot \frac{d^2 W_z}{dz^2} = M_z, \tag{2}$$

where $D = \frac{E \cdot I}{1 - \nu^2}$ is cylindrical stiffness.

Differentiating twice both sides of equation (2) with respect to z and denoting it $\frac{d^2 M_z}{dz^2} = g(z)$, it takes the form:

$$D \cdot \frac{d^4 W_z}{dz^4} = g(z). \tag{3}$$

Proceeding from the assumption of rigid embedding of the beam at the support point, the expression for determining the segment deformations will take the form:

$$W_z = \frac{1}{D} \int \int \int \int g(z) \cdot dz. \tag{4}$$

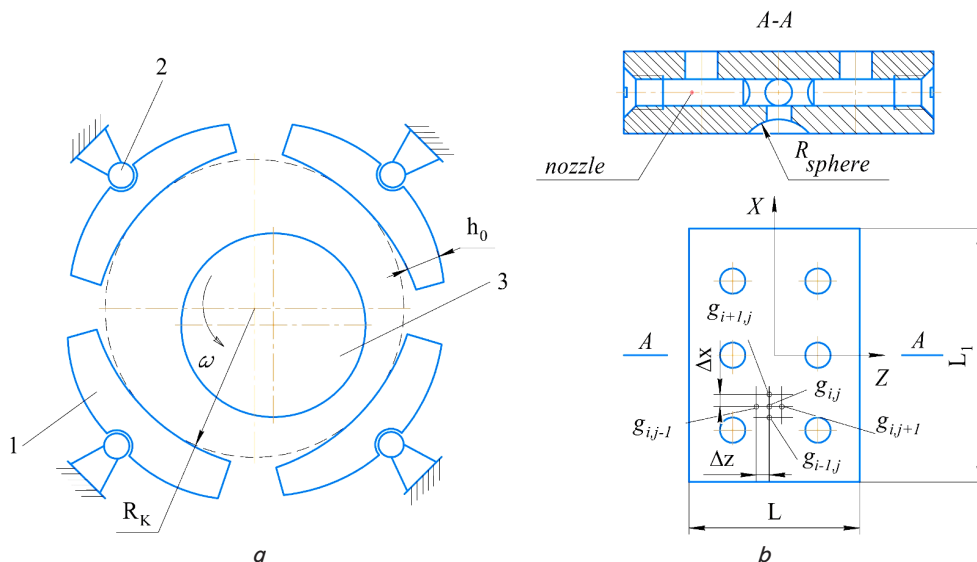


Fig. 1. Diagram of a segmental-type hydrostatic bearing: a – general view of the bearing; b – working surface of a segment with spherical bearing chambers

To determine the distributed load g_{ij} , the Reynolds equation was used:

$$\frac{\partial}{\partial x} \left(h^3 \frac{\partial g}{\partial x} \right) + \frac{\partial}{\partial z} \left(h^3 \frac{\partial g}{\partial z} \right) = 6\mu \cdot \omega \cdot R \frac{dh}{dx},$$

where h is the bearing clearance; g is distributed load; x, z are coordinate axes (circumferential and axial, respectively); μ is the dynamic viscosity of the working fluid; R is the shaft radius.

Using a five-point template (Fig. 1, b), the difference notation of the Reynolds equation takes the form:

$$r_{2i} \cdot g_{i+1,j} + r_{3i} \cdot g_{i,j} + r_{4i} \cdot g_{i-1,j} = F_i - r_{1i} \cdot g_{i,j+1} - r_{1i} \cdot g_{i,j-1},$$

where

$$r_{1i} = \frac{h_i^3}{\Delta z^2}; r_{2i} = \frac{h_i}{\Delta x^2} + \frac{3 \cdot h_i^2}{4 \cdot \Delta x^2} \cdot (h_{i+1} - h_{i-1});$$

$$r_{3i} = -\frac{2 \cdot h_i^3}{\Delta x^2} - \frac{2 \cdot h_i^3}{\Delta z^2}; r_{4i} = \frac{h_i^3}{\Delta x^2} - \frac{3 \cdot h_i^2}{4 \cdot \Delta x^2} \cdot (h_{i+1} - h_{i-1}).$$

To solve the difference scheme of the Reynolds equation written in an implicit form, the well-known transverse-longitudinal sweep method was applied. In this case, along with the basic values g_n and g_{n+1} of the sought grid function, introduce an intermediate value $g_{n+1/2}$ in the sublayer. Perform a transition from the n -th layer to the $n+1$ -th layer in two stages:

1. Formulas of transition from the n -th layer to the $n+1/2$ -nd layer (transverse run):

$$(g_{i,j})_{n+1/2} = \alpha_{1i,j} \cdot (g_{i+1,j})_{n+1/2} + \beta_{1i,j},$$

where $\alpha_{1i,j}$, and $\beta_{1i,j}$ are the run coefficients;

$$\alpha_{1i,j} = -\frac{A_{1i}}{B_{1i} + C_{1i} \cdot \alpha_{1i-1,j}}; \beta_{1i,j} = \frac{F_{1i} - C_{1i} \cdot \beta_{1i-1,j}}{B_{1i} + C_{1i} \cdot \alpha_{1i-1,j}};$$

A_{1i}, B_{1i}, C_{1i} and F_{1i} are constant coefficients; $A_{1i}=r_{2i}; B_{1i}=r_{3i}; C_{1i}=r_{4i}; F_{1i}=F_i - r_{1i}(g_{i,j+1})_n - r_{1i}(g_{i,j-1})_n$.

2. Formulas for the transition from the $n+1/2$ -th layer to the n -th layer (longitudinal run):

$$(g_{i,j})_{n+1} = \alpha_{2i,j} \cdot (g_{i,j+1})_{n+1} + \beta_{2i,j},$$

where $\alpha_{2i,j}$ and $\beta_{2i,j}$ are the run coefficients;

$$\alpha_{2i,j} = -\frac{A_{2i}}{B_{2i} + C_{2i} \cdot \alpha_{2i,j-1}}; \beta_{2i,j} = \frac{F_{2i} - C_{2i} \cdot \beta_{2i,j-1}}{B_{2i} + C_{2i} \cdot \alpha_{2i,j-1}};$$

$A_{2i}=r_{1i}; B_{2i}=r_{3i}; C_{2i}=r_{1i}; F_{2i}=F_i - r_{2i}(g_{i+1,j})_{n+1/2} - r_{4i}(g_{i-1,j})_{n+1/2}$.

Using the method of trapezoids, the load distributed over the surface was replaced by a linear load along the Z axis:

$$g_j = \Delta x \cdot \sum_{i=1}^{N_1} g_{i,j},$$

where N_1 is the number of grid nodes from the segment support to the edge (X -axis); $j=2, \dots, N_2-1$; N_2 is the number of grid points from the segment support to the edge (Z -axis).

After replacing the linear load g_j with an averaged constant linear load, the equation for its determination takes the form:

$$g_{jcp} = \frac{1}{N_2} \cdot \sum_{j=2}^{N_2-1} g_j.$$

Afterward, the transformations, the expression for numerical determination of deformations in the axial direction takes the form:

$$W_{zj} = \frac{g_{jcp} \cdot z_j^4}{24 \cdot D} = \frac{g_{jcp} \cdot [\Delta z \cdot (j-1)]^4}{24 \cdot D}, \tag{5}$$

where $j=1, \dots, N_2$.

To determine the segment deformations in the circumferential direction, the basic equation was adopted as the initial equation to determine deformations of rods with a curved axis under the action of forces in the curvature plane [15]:

$$\frac{d^2 W_x}{d\theta^2} + W_x = \frac{M_x \cdot R_k^2}{E \cdot I}, \tag{6}$$

W_x is the deformation of the segment in a circumferential direction; R_k is the radius of the segment curvature; θ is the current angle measured from the segment edge and varying from 0 to φ ; φ is the angle defining the part of the segment between its edge and the support; M_x is the bending moment; E is the modulus of elasticity of the segment material; I is the moment of inertia of the segment section perpendicular to the circumferential coordinate.

After substitution of the expression for the moment:

$$M_x = R_k^2 \cdot \theta \cdot g(x) \cdot \sin \frac{\theta}{2},$$

equation (6) takes the form:

$$\frac{d^2 W_x}{d\theta^2} + W_x = K_1 \cdot \theta \cdot \sin \frac{\theta}{2}, \tag{7}$$

where $K_1 = \frac{g(x) \cdot R_k^4}{E \cdot I}$; $g(x)$ is the load distributed over the working surface of the segment.

The expression for the averaged constant linear load along the X axis takes the form:

$$g_{icp} = \frac{\Delta z}{N_1} \sum_{i=2}^{-1} \sum_{j=2}^{-1} g_{ij}.$$

Equation (7) is inhomogeneous. Its general solution gives a sum of the general solution of the corresponding homogeneous equation and the partial solution of the inhomogeneous linear equation:

$$W_x = W_{x1} + W_{x2}. \tag{8}$$

General solution of W_{x1} of the homogeneous equation $W''_x + W_x = 0$ takes the form [16]:

$$W_{x1} = C_{10} \cdot C_{10} \theta + C_{11} \cdot \sin \theta. \tag{9}$$

To find a partial solution of W_{x2} of the inhomogeneous equation (7), the characteristic equation $K_2^2 + 1 = 0$, was compiled whence $K_2 = \sqrt{-1} = i$.

The solution was found as in [16]:

$$W_{x2} = x^p \cdot e^{ax} \cdot [Q_1(x) \cdot \cos(b \cdot x) + Q_2(x) \cdot \sin(b \cdot x)], \tag{10}$$

where $Q_1(x)$ and $Q_2(x)$ are polynomials of degree « m » with inhomogeneous coefficients; p is the multiplicity of the root of the characteristic equation equal to $a+b \cdot i$.

In this case, $a=0$; $b=1/2$; $p=0$ because $1/2i$ is not a root of the characteristic equation $K_2^2+1=0$.

In this case, a partial solution of the inhomogeneous equation will take the form:

$$W_{x2} = (A_1 \cdot \theta + B_1) \cdot \sin \frac{\theta}{2} + (A_2 \cdot \theta + B_2) \cdot \cos \frac{\theta}{2}. \quad (11)$$

When differentiating expression (11) twice and substituting this expression in (7), the following equation was obtained:

$$\left(-A_2 - \frac{A_1 \cdot \theta}{4} - \frac{B_1}{4}\right) \cdot \sin \frac{\theta}{2} + \left(A_1 - \frac{A_2 \cdot \theta}{4} - \frac{B_2}{4}\right) \cdot \cos \frac{\theta}{2} + (A_1 \cdot \theta + B_1) \cdot \sin \frac{\theta}{2} + (A_2 \cdot \theta + B_2) \cdot \cos \frac{\theta}{2} = K_1 \cdot \theta \cdot \sin \frac{\theta}{2}.$$

Comparing the coefficients in both sides of the equality, we will have:

$$A_1 = \frac{4}{3} \cdot K_1; B_1 = 0; A_2 = 0; B_2 = -\frac{16}{9} \cdot K_1.$$

Partial solution in this case will take the form:

$$W_{x2} = \frac{4}{3} \cdot K_1 \cdot \theta \cdot \sin \frac{\theta}{2} - \frac{16}{9} \cdot K_1 \cdot \cos \frac{\theta}{2}. \quad (12)$$

A general solution to the inhomogeneous equation (7) takes the form:

$$W_x = C_{10} \cdot \cos \theta + C_{11} \cdot \sin \theta + \frac{4}{3} \cdot K_1 \cdot \theta \cdot \sin \frac{\theta}{2} - \frac{16}{9} \cdot K_1 \cdot \cos \frac{\theta}{2}. \quad (13)$$

Arbitrary constants C_{10} and C_{11} are found from the condition of segment anchoring:

$$(W_x)_{\theta=\varphi} = 0; \left(\frac{dW_x}{d\theta}\right)_{\theta=\varphi} = 0. \quad (14)$$

Using expressions (13), equations were written for arbitrary constants C_{10} and C_{11} :

$$C_{11} = -\frac{2}{3} \cdot K_1 \cdot \varphi \cdot \cos \frac{\varphi}{2} \cdot (2 - \cos \varphi) - \frac{4}{3} \cdot K_1 \cdot \sin \frac{\varphi}{2} \cdot (\cos \varphi - 4),$$

$$C_{10} = \frac{K_1}{\cos \varphi} \left[\frac{16}{9} \cdot \cos \frac{\varphi}{2} - \frac{4}{3} \cdot \varphi \cdot \sin \frac{\varphi}{2} + \frac{4}{3} \cdot \sin \varphi \cdot \left(\varphi \cdot \cos \frac{\varphi}{2} - \frac{4}{3} \cdot \sin \frac{\varphi}{2} \right) - \frac{\sin 2\varphi}{3} \cdot \left(\varphi \cdot \cos \frac{\varphi}{2} - \frac{2}{3} \cdot \sin \frac{\varphi}{2} \right) \right]. \quad (15)$$

Expressions (13) and (15) describe deformations of the segment in the circumferential direction. At $\theta=0$, the value of the segment deformation will be maximum and equal to:

$$W_{x\max} = C_{10} - \frac{16}{9} \cdot K_1. \quad (16)$$

Elastic deformations of the segments were calculated using expressions (5), (13), and (15). Deformations were calculated for the most loaded lower segment in which pressure in the chambers at large eccentricities was close to the feeding pressure of the working fluid. The pressure diagram over the working surface of the segment was determined from the joint solution of the Reynolds equations and the flow rate balance. Elastic deformations of the segment were calculated for a segmental hydrostatic bearing having the following basic dimensions:

1. Bearing diameter $D=60$ mm.
2. Bearing length $L=60$ mm.
3. Radial clearance between the shaft and the bearing $\delta_0=0.08$ mm.
4. Diameter of the nozzles installed at the inlet to the chambers $d_0=1$ mm.
5. The number of segments $k=4$.
6. Shaft weight $G=40$ kg.
7. Circumferential length of the segment $L_1=45$ mm.
8. Segment thickness $h_0=16$ mm.

The results obtained in calculating elastic deformations of the segment in the circumferential direction at various pressures P of the working fluid feed are shown in Fig. 2. Values of elastic deformations of the segment in the axial direction at various values of the feeding pressure are shown in Fig. 3.

Fig. 4 shows the character of change in the segment deformation in a circumferential direction for various segment materials. The character of the deformation change is linear.

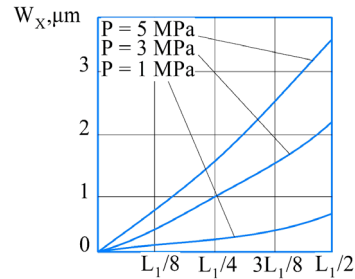


Fig. 2. Deformation of the segment in the circumferential direction

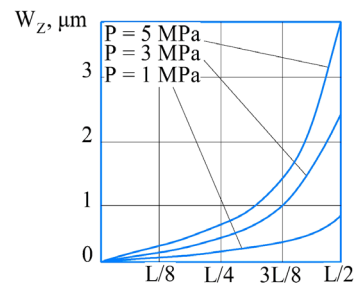


Fig. 3. Deformations of the segment in the axial direction

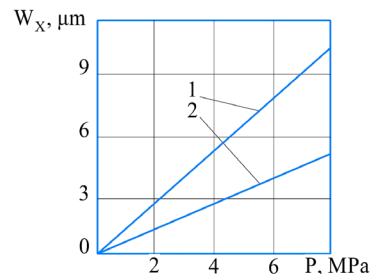


Fig. 4. Deformations of the segment manufactured of different materials: 1 – bronze; 2 – steel

With a working fluid feed pressure of 6 MPa, the transition of the extreme point measured 5.3 % of the radial clearance for a steel segment and 10.5 % i. e. about 2 times more for a bronze segment at the same pressures.

Quantitative assessment of elastic deformation of the segment and influence of the working fluid feed pressure on it as applied to hydrostatic bearings is a novelty.

5. 2. Determining the segment thickness and the amount of deformation of its spherical support

To determine the segment thickness, a differential equation of a curved beam [15] was used:

$$\frac{d^2W_x}{d\theta^2} = \frac{M_x \cdot R_k^2}{E \cdot I} \tag{17}$$

After double integration, equation (17) takes the form:

$$W_x = -2 \cdot K_1 \cdot \left(2 \cdot \theta \cdot \sin \frac{\theta}{2} + 4 \cdot \cos \frac{\theta}{2} \right) + C_{12} \cdot \theta + C_{13} \tag{18}$$

Arbitrary constants were written proceeding from the conditions of segment fixation (14):

$$C_{12} = 2 \cdot K_1 \cdot \left(\varphi \cdot \cos \frac{\varphi}{2} + 2 \cdot \sin \frac{\varphi}{2} \right),$$

$$C_{13} = 8 \cdot K_1 \cdot \varphi \cdot \sin \frac{\varphi}{2} + 2 \cdot K_1 \cdot (8 - \varphi^2) \cdot \cos \frac{\varphi}{2} \tag{19}$$

An expression was written using equations (18) and (19) to determine the segment thickness h_0 :

$$h_0 = \sqrt[3]{\frac{12 \cdot g_{icp} \cdot R_k^4 \cdot (m_1 + m_2)}{L \cdot E \cdot W_x}} \tag{20}$$

where

$$m_1 = -2 \cdot \left(2 \cdot \theta \cdot \sin \frac{\theta}{2} + 4 \cdot \cos \frac{\theta}{2} \right) + 2 \cdot \left(\varphi \cdot \cos \frac{\varphi}{2} + 2 \cdot \sin \frac{\varphi}{2} \right) \cdot \theta;$$

$$m_2 = 8 \cdot \varphi \cdot \sin \frac{\varphi}{2} + 2(8 - \varphi^2) \cdot \cos \frac{\varphi}{2}.$$

To determine the deformation of spherical supports of the segments, a formula of change in volume of a solid steel ball subjected to uniform pressure was used [17]:

$$\Delta_1 = -\frac{3 \cdot P \cdot (1 - 2 \cdot \nu)}{E} \tag{21}$$

where P is specific pressure on the sphere; Δ_1 is relative volumetric compression; ν is Poisson's ratio; E is the modulus of elasticity of the spherical support material.

If we denote the diameter of the spherical support before deformation by d and the diameter after deformation by d_1 , then a decrease in the spherical support volume can be calculated from the dependence $\frac{\pi \cdot d^3}{6} \cdot \Delta_1$. Volume after deformation can be found from the dependence:

$$\frac{\pi \cdot d^3}{6} - \frac{\pi \cdot d_1^3}{6} \cdot \Delta_1 = \frac{\pi \cdot d_1^3}{6} \tag{22}$$

whence $d_1 = d \cdot \sqrt[3]{1 - \Delta_1}$.

The amount of deformation of the spherical support of the segment is determined from the dependence:

$$\Delta = d - d_1 = d \cdot \left(1 - \sqrt[3]{1 - \Delta_1} \right) \tag{23}$$

The thickness of the segment and deformation of its spherical support were determined using expressions (20) and (23).

Having determined the thickness of the segment with the minimum allowable value of its deformation, it is possible to neglect the deformability of the segments when determining the main characteristics of the segmental hydrostatic bearing.

In order that the magnitude of displacement of extreme points of the segment not to exceed 0.5 % of the radial clearance of 80 μm at different values of the feeding pressure, different thicknesses of the segments h_0 is required.

Using expression (20), it was found (Fig. 5) that with an increase in the feed pressure from 1 to 10 MPa, in order to ensure a given amount of displacement, it is necessary to increase the thickness of the steel segment from 16 to 36.5 mm, i.e. more than 2 times. When the feeding pressure changes from 1 MPa to 10 MPa, the increase in thickness of the bronze segment is more than 3 times in comparison with the steel segment.

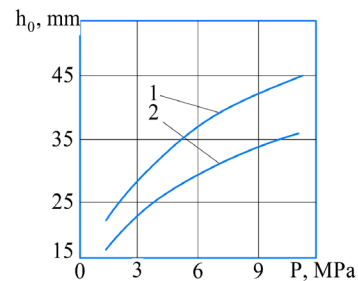


Fig. 5. Influence of the working fluid feed pressure on the segment thickness: 1 – a segment of bronze; 2 – a segment of steel

Using expression (23), it was found (Fig. 6) that the value of deformability of the spherical support of the segment depends significantly on the feeding pressure and the material used.

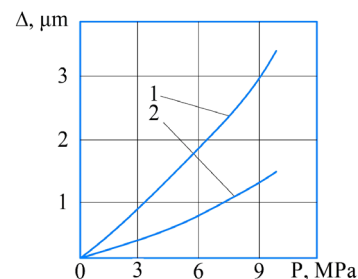


Fig. 6. Influence of the feed pressure on deformation of the spherical support: 1 – a segment of bronze; 2 – a segment of steel

The dependence of deformation of the spherical support on the feeding pressure is nonlinear.

6. Discussion of the results obtained in the study of the deformation of segments and their spherical supports

The results obtained in calculating the deformation of segments and their spherical supports are shown in Fig. 2–6.

It can be seen from Fig. 2 that the greatest displacements caused by segment deformation are made by the extreme point of the segment. This suggests that the developed mathematical model qualitatively correctly describes the segment

deformation. For a feeding pressure $P=1$ MPa, displacement of the extreme segment point is approximately 0.9 % of radial clearance of 80 μm . With an increase in the feeding pressure to $P=5$ MPa, displacement of the extreme point as a result of segment deformation is approximately 4.5 % of radial clearance and, therefore, can have a significant effect on the main characteristics of the segmental hydrostatic bearing.

It can be seen from Fig. 3 that the greatest displacements caused by deformation are found for the extreme point of the segment. The character of deformation change along the segment axis is substantially nonlinear and nonlinearity increases with an increase in the feeding pressure of the working fluid. Quantitative assessment of the deformation shows that with an increase in the feeding pressure from 1 MPa to 5 MPa, displacement of the segment's extreme point increased by about 5 times.

Linear character of change in segment deformation in circumferential direction was revealed for various segment materials (Fig. 4).

It was found that the value of the working fluid feed pressure significantly affects the thickness of the segment (Fig. 5). With an increase in the feeding pressure from 1 MPa to 10 MPa, the thickness of the steel segment increases more than 2 times and the thickness of the bronze segment increases more than 3 times.

It can be seen from Fig. 6 that deformation of the spherical support can have a significant effect on the bearing clearance, and, consequently, on its main characteristics. For example, deformation of the steel spherical support is approximately 2.1 % of the radial clearance at feeding pressure of 10 MPa, and deformation of the bronze spherical support is 4.2 % of the radial clearance at the same pressure.

As a result of the analysis of deformation of the segment and its spherical support, it can be noted that total clearance between the shaft and the bearing increases significantly because of segment deformation at certain pressures of the working fluid feed. It becomes necessary to take these deformations into account when calculating the basic characteristics of the bearing. The materials adopted for the segment and its spherical support also have a significant effect on the total bearing clearance.

Determining the segment thickness with the minimum allowable value of its deformation makes it possible to design the segmental hydrostatic bearings more rationally.

The proposed solutions and the results obtained make it possible to solve the problem of deformation of segments and

their spherical supports by a computational method that was absent in existing studies. Determination of deformation of the segments and their spherical bearings will also enable a more accurate characterization of the hydrostatic segmental bearing.

The advantage of this study consists in an integrated approach associated with solving a complex hydrodynamic problem and taking into account the deformation of segments and their spherical supports.

The limitations inherent in this study are primarily related to the disregard for temperature deformation of the segments. Not taking into account temperature deformations in this study was substantiated by the fact that operation of hydrostatic bearings is associated with high flow rates of the working fluid and a very small increase in temperature in the bearing. Experimental studies have also shown that the temperature of the working fluid practically does not change during the bearing operation. However, it may be necessary to take into account thermal deformations for powerful turbines with a large bearing surface.

The disadvantage of this study consists in the lack of experimental confirmation of the results obtained. Therefore, it is necessary to conduct further experimental studies to assess the elastic deformation of segments and their spherical supports and confirm the theoretical studies obtained.

7. Conclusions

1. It was revealed that the magnitude of influence of pressure of the working fluid feed on maximum deformation of the segment with an increase in pressure to 5 MPa is approximately 4.5 % of the radial clearance and can affect the bearing characteristics. A substantially nonlinear character of deformation along the segment axis was revealed.

2. It was found that the value of the working fluid feed pressure substantially affects the segment thickness. With the growth of feed pressure from 1 MPa to 10 MPa, required thickness increases from 16 mm to 36.5 mm, i.e. more than 2 times for the steel segment and more than 3 times for the bronze segment. It was also found that the pressure of the working fluid can have a substantial effect on the deformation of the spherical support of the segment and on the bearing clearance. So, at a feeding pressure of 10 MPa and higher, deformation is 2.1 % of the radial clearance for steel spherical support and 4.2 % for bronze spherical support and can affect the bearing characteristics.

References

- Hu, Z., Wang, Z., Huang, W., Wang, X. (2019). Supporting and friction properties of magnetic fluids bearings. *Tribology International*, 130, 334–338. doi: <https://doi.org/10.1016/j.triboint.2018.10.006>
- Xu, H., Yang, J., Gao, L., An, Q. (2020). The influences of bump foil structure parameters on the static and dynamic characteristics of bump-type gas foil bearings. *Proceedings of the Institution of Mechanical Engineers, Part J: Journal of Engineering Tribology*, 234 (10), 1642–1657. doi: <https://doi.org/10.1177/1350650120912609>
- Koosha, R., San Andrés, L. (2020). A Computational Model for the Analysis of the Static Forced Performance of Self-Equalizing Tilting Pad Thrust Bearings. *Journal of Engineering for Gas Turbines and Power*, 142 (10). doi: <https://doi.org/10.1115/1.4048458>
- Xiang, G., Han, Y., He, T., Wang, J., Xiao, K., Li, J. (2020). Wear and fluid-solid-thermal transient coupled model for journal bearings. *Applied Mathematical Modelling*, 85, 19–45. doi: <https://doi.org/10.1016/j.apm.2020.03.037>
- Santos, I. (2018). Controllable Sliding Bearings and Controllable Lubrication Principles – An Overview. *Lubricants*, 6 (1), 16. doi: <https://doi.org/10.3390/lubricants6010016>
- EL-Said, A. K., EL-Souhily, B. M., Crosby, W. A., EL-Gamal, H. A. (2017). The performance and stability of three-lobe journal bearing textured with micro protrusions. *Alexandria Engineering Journal*, 56 (4), 423–432. doi: <https://doi.org/10.1016/j.aej.2017.08.003>

7. Summer, F., Bergmann, P., Grün, F. (2017). Damage Equivalent Test Methodologies as Design Elements for Journal Bearing Systems. *Lubricants*, 5 (4), 47. doi: <https://doi.org/10.3390/lubricants5040047>
8. Zernin, M. V., Mishin, A. V., Rybkin, N. N., Shil'ko, S. V., Ryabchenko, T. V. (2017). Consideration of the multizone hydrodynamic friction, the misalignment of axes, and the contact compliance of a shaft and a bush of sliding bearings. *Journal of Friction and Wear*, 38 (3), 242–251. doi: <https://doi.org/10.3103/s1068366617030163>
9. Zhang, J., Tan, A., Spikes, H. (2016). Effect of Base Oil Structure on Elastohydrodynamic Friction. *Tribology Letters*, 65 (1). doi: <https://doi.org/10.1007/s11249-016-0791-7>
10. Villaverde, R. (2016). Base isolation with sliding hydromagnetic bearings: concept and feasibility study. *Structure and Infrastructure Engineering*, 13 (6), 709–721. doi: <https://doi.org/10.1080/15732479.2016.1187634>
11. Polyakov, R., Savin, L., Fetisov, A. (2018). Analysis of the conditions for the occurrence of the effect of a minimum of friction in hybrid bearings based on the load separation principle. *Proceedings of the Institution of Mechanical Engineers, Part J: Journal of Engineering Tribology*, 233 (2), 271–280. doi: <https://doi.org/10.1177/1350650118777143>
12. Schüller, E., Berner, O. (2021). Improvement of Tilting-Pad Journal Bearing Operating Characteristics by Application of Eddy Grooves. *Lubricants*, 9 (2), 18. doi: <https://doi.org/10.3390/lubricants9020018>
13. Kukla, S., Buchhorn, N., Bender, B. (2016). Design of an axially concave pad profile for a large turbine tilting-pad bearing. *Proceedings of the Institution of Mechanical Engineers, Part J: Journal of Engineering Tribology*, 231 (4), 479–488. doi: <https://doi.org/10.1177/1350650115592919>
14. Artemenko, N. P., Nazin, V. I. (1982). Raschet karakteristik mnogosegmentnyh gidrostaticheskikh podshipnikov s tochechnymi kamerami. *Issledovanie gidrostaticheskikh opor i uplotneniy dvigateley letatel'nyh apparatov*, 1, 12–22.
15. Timoshenko, S. P. (1972). *Kurs teorii uprugosti*. Kyiv: Naukova dumka, 832.
16. Korn, G., Korn, T. (1974). *Spravochnik po matematike*. Moscow: Nauka, 832.
17. Timoshenko, S. P., Lessel's, Dzh. (1931). *Prikladnaya teoriya uprugosti*. Leningrad: Gostekhizdat, 394.